6-12-2018

The Allowed Parameter Space of a Long-lived Neutron Star as the Merger Remnant of GW170817

Shunke Ai
Beijing Normal University

He Gao
Beijing Normal University, gaohe@bnu.edu.cn

Zi-Gao Dai
Nanjing University, dzg@nju.edu.cn

Xue-Feng Wu
Chinese Academy of Sciences, xfwu@pmo.ac.cn

Ang Li
Xiamen University, liang@xmu.edu.cn

Follow this and additional works at: https://digitalscholarship.unlv.edu/physastr_fac_articles

See next page for additional authors

Part of the Astrophysics and Astronomy Commons

Authors

Shunke Ai, He Gao, Zi-Gao Dai, Xue-Feng Wu, Ang Li, Bing Zhang, and Mu-Zi Li

The Allowed Parameter Space of a Long-lived Neutron Star as the Merger Remnant of GW170817

Shunke Ai[1] , He Gao[1] , Zi-Gao Dai[2,3] , Xue-Feng Wu[4] , Ang Li[5] , Bing Zhang[6,7,8] , and Mu-Zi Li[1]

[1] Department of Astronomy, Beijing Normal University, Beijing 100875, People's Republic of China; gaohe@bnu.edu.cn
[2] School of Astronomy and Space Science, Nanjing University, Nanjing 210093, People's Republic of China; dzg@nju.edu.cn
[3] Key Laboratory of Modern Astronomy and Astrophysics (Nanjing University), Ministry of Education, People's Republic of China
[4] Purple Mountain Observatory, Chinese Academy of Sciences, Nanjing 210008, People's Republic of China; xfwu@pmo.ac.cn
[5] Department of Astronomy, Xiamen University, Xiamen, Fujian 361005, People's Republic of China; liang@xmu.edu.cn
[6] Department of Physics and Astronomy, University of Nevada Las Vegas, Las Vegas, NV 89154, USA; zhang@physics.unlv.edu
[7] Department of Astronomy, School of Physics, Peking University, Beijing 100871, People's Republic of China
[8] Kavli Institute of Astronomy and Astrophysics, Peking University, Beijing 100871, People's Republic of China

Abstract

Due to the limited sensitivity of the current gravitational wave (GW) detectors, the central remnant of the binary neutron star (NS) merger associated with GW170817 remains an open question. In view of the relatively large total mass, it is generally proposed that the merger of GW170817 would lead to a short-lived hypermassive NS or directly produce a black hole (BH). There is no clear evidence to support or rule out a long-lived NS as the merger remnant. Here, we utilize the GW and electromagnetic (EM) signals to comprehensively investigate the parameter space that allows a long-lived NS to survive as the merger remnant of GW170817. We find that for some stiff equations of state, the merger of GW170817 could, in principle, lead to a massive NS, which has a millisecond spin period. The post-merger GW signal could hardly constrain the ellipticity of the NS. If the ellipticity reaches 10^{-3}, in order to be compatible with the multi-band EM observations, the dipole magnetic field of the NS (B_p) is constrained to the magnetar level of $\sim 10^{14}$ G. If the ellipticity is smaller than 10^{-4}, B_p is constrained to the level of $\sim 10^9$–10^{11} G. These conclusions weakly depend on the adoption of the NS equation of state.

Key words: gamma-ray burst: general – gravitational waves

1. Introduction

On 2017 August 17, the LIGO-Virgo scientific collaboration for the first time detected a gravitational wave (GW) signal from a binary neutron star (NS) merger event (i.e., GW170817; Abbott et al. 2017a). Multi-wavelength electromagnetic (EM) counterparts to GW170817 have also been detected (see Abbott et al. 2017b for a summary).

Comprehensive analyses of the multi-messenger information have provided some important physical properties of the binary system and the merger process for GW170817. For instance, the host galaxy of the system was identified as NGC 4993 (Coulter et al. 2017), an early-type S0 galaxy with redshift $z = 0.0097$ (de Vaucouleurs et al. 1991). The chirp mass of the binary system is determined to be $1.188^{+0.004}_{-0.002}\,M_\odot$, and the mass ratio of the two NSs was constrained to be in the range of 0.4–1.0 (Abbott et al. 2017a),[9] so that the total mass of the system would be $2.74\,M_\odot$ and the component mass of the binary system would be between $0.86\,M_\odot$ and $2.26\,M_\odot$ (Abbott et al. 2017a).

During the merger, a small fraction of baryonic matter is ejected, including a lanthanide-free disk wind ejecta with mass $M_{\rm ej,blue} \approx 0.01$–$0.04\,M_\odot$, and initial speed $\beta_{\rm i,blue} \approx 0.2$–$0.3$ (Chornock et al. 2017; Cowperthwaite et al. 2017; Gao et al. 2017a; Kasen et al. 2017; Kilpatrick et al. 2017; Shappee et al. 2017; Tanvir et al. 2017; Villar et al. 2017), and a lanthanide-rich dynamical ejecta[10] (tidally ripped and dynamically

launched matter) with mass $M_{\rm ej,red} \approx 0.03$–$0.05\,M_\odot$ and initial speed $\beta_{\rm i,red} \approx 0.1$–$0.2$ (Arcavi et al. 2017; Cowperthwaite et al. 2017; Drout et al. 2017; Evans et al. 2017; Gao et al. 2017a; Kasen et al. 2017; Kilpatrick et al. 2017; Nicholl et al. 2017; Smartt et al. 2017; Villar et al. 2017). Such ejected matter powered an ultraviolet/optical/near-infrared counterpart following GW170817, named AT2017gfo (see Metzger 2017 for a review).

The remaining matter would settle to form a new central compact object fed by an accretion disk, so that a relativistic jet was launched. When propagating through the surrounding ejecta, the jet could be structured (Kasliwal et al. 2017; Gottlieb et al. 2017; Lazzati et al. 2017; Mooley et al. 2017; Piro & Kollmeier 2017; Xiao et al. 2017; Zhang et al. 2018; Lyman et al. 2018). Internal and external dissipation of the structured jet gives rise to multi-band EM emissions, including a short duration gamma-ray burst detected by the Fermi Gamma-ray Burst Monitor (GRB 170817) (Goldstein et al. 2017), and late time brightening afterglow signals in the X-ray, optical and radio bands (Lazzati et al. 2017; Troja et al. 2017, 2018; Margutti et al. 2018; Meng et al. 2018). Considering that the peak isotropic luminosity of GRB 170817A ($\sim 1.7 \times 10^{47}$ erg s^{-1}) is abnormally low compared with other short GRBs (Goldstein et al. 2017; Zhang et al. 2018), the late afterglow signals are relatively weak, and the rising slope of the afterglow signals is relatively small. A large binary inclination angle ($\sim 20°$) relative to our line of sight is inferred (Lazzati et al. 2017; Mooley et al. 2017; Lyman et al. 2018), which is well consistent with the results from the GW signal analyses (Abbott et al. 2017b).

What is the central remnant of GW170817 remains an open question. Considering that the total mass of the GW170817 binary system is relatively large ($2.74\,M_\odot$), it is generally

---

[9] With the information of the optical/infrared (IR) counterpart, Gao et al. (2017a) placed a more stringent constraint on the mass ratio of GW170817 system to the range of 0.46–0.67.

[10] The opposite view of interpreting the blue component as due to the dynamical ejecta also exists in the literature (e.g., Kasen et al. 2017; Nicholl et al. 2017).

proposed that the merger of GW170817 would lead to a temporal hypermassive NS (supported by differential rotation) which survived 10–100 ms before collapsing into a black hole (BH) or even a BH directly (Bauswein et al. 2017; Ma et al. 2017; Margalit & Metzger 2017; Perego et al. 2017; Ruiz et al. 2017; Metzger et al. 2018; Rezzolla et al. 2018). However, our poor knowledge about the NS equation of state (EoS) makes the discussion more complex. For instance, as long as the NS EoS is stiff enough, the merger remnant of GW170817 could be a long-lived massive NS, as argued early by Dai & Lu (1998a) and Dai et al. (2006), and within such a scenario, the multi-band data of AT2017gfo could be also reproduced (Yu & Dai 2017; Li et al. 2017b). Assuming that the merger remnant is a long-lived NS, a considerable mass would be still ejected by a neutrino-driven or viscosity-driven wind (e.g., Metzger et al. 2018; Radice et al. 2018), which is discussed as an alternative mass source for the blue kilonova.

In principle, post-merger GW signals could be used to probe the property of the remnant. But the search for post-merger GWs of GW170817 only provides an upper limit of the characteristic amplitude, mainly limited by the current sensitivity of the LIGO/Virgo detectors (Abbott et al. 2017c). In this case, we can only rely on the information of the EM signals to make constraints. It has long been proposed that when the merger remnant is a long-lived massive NS, more abundant EM signatures are expected (Dai & Lu 1998a, 1998b; Dai 2004; Dai et al. 2006; Fan et al. 2013; Gao et al. 2013, 2015, 2017b; Yu et al. 2013; Zhang 2013; Metzger & Piro 2014; Wu et al. 2014; Li & Yu 2016; Siegel & Ciolfi 2016a, 2016b; Sun et al. 2017). For instance, after the relativistic jet propagates through the surrounding ejecta, a Poynting-flux outflow from the NS could leak out to power an extended emission through its dissipation at a large radius (Dai 2004; Zhang 2013; Rowlinson et al. 2014; Lü et al. 2015; Sun et al. 2017). Due to the dynamical motion of the ejecta, the ejecta materials tend to quench the outflow by closing the gap, so that the Poynting-flux outflow would be trapped inside. The outflow could then inject extra energy into the ejecta to increase its internal energy and kinetic energy, either via direct energy injection by a Poynting flux (Bucciantini et al. 2012), or due to heating from the bottom by the photons generated in a dissipating magnetar wind via magnetic reconnection or self-dissipation (Zhang 2013). The heated ejecta material would power a bright thermal emission component (Yu et al. 2013; Metzger & Piro 2014), normally brighter than the radioactively driven kilonova (Li & Paczyński 1998; Metzger et al. 2010). Nevertheless, the accelerated ejecta materials might also give rise to strong afterglow emission by driving a strong forward shock into an ambient medium (Gao et al. 2013). When the ejecta becomes optically thin, if the massive NS still survives, the dissipated photons from its Poynting-flux outflow would eventually diffuse out, resulting in a late time re-brightening X-ray signal (Metzger & Piro 2014; Gao et al. 2015, 2017b; Sun et al. 2017).

In this paper, we utilize the GW and electromagnetic (EM) signals to comprehensively investigate the possibility of a long-lived massive NS as the merger remnant of GW170817, and give constraints on the physical properties of the NS, if it exists.

2. NS EoS

For GW170817, the total gravitational mass of the binary system is estimated as $2.74\,M_{\odot}$ (Abbott et al. 2017a). Numerical simulations show that after the merger process and

differential rotation phase, the mass of the uniformly rotating remnant could be estimated as (Hanauske et al. 2017; Rezzolla et al. 2018)

$$M_{\mathrm{ur}} = \delta M_g - \lambda^{-1} M_{\mathrm{ej}}, \qquad (1)$$

where M_g is the initial gravitational mass of the merger remnant, δ is the mass fraction of the core after dynamical mass ejection, $\lambda = 1.17$ is the numerical ratio of the baryonic mass and the gravitational mass (Rezzolla et al. 2018), and M_{ej} is the mass of the ejecta from the core. According to Hanauske et al. (2017), δ ranges from 0.9 to 1 (with an average value of 0.95), depending on the adoption of EoS and the initial configuration or other properties of the NS–NS system. On the other hand, M_{ej} also has a large uncertainty, especially when the central remnant is a long-lived NS. Here, we adopt $\delta = 0.95$ and associate M_{ej} with the blue kilonova ejecta mass $M_{\mathrm{ej}} \sim 0.02\,M_{\odot}$ (Metzger 2017). To be conservative, we also test different situations with δ ranging from 0.9 to 1, and M_{ej} ranging from $0.01\,M_{\odot}$ to $0.04\,M_{\odot}$. We find that once the EoS is stiff enough to support a long-lived NS, the uncertainty of the core mass mainly affects the constraint on the spin of the long-lived NS, but only slightly affects the constraint on other NS properties, such as the NS dipole magnetic field strength (see Section 4 for details).

Before the merger, the two NSs are in the Keplerian orbits, so the post-merger central remnant must be rapidly spinning. The rapid rotation could enhance the maximum gravitational mass (M_{max}) allowed for NS survival, where M_{max} can be parameterized as (Lasky et al. 2014)

$$M_{\mathrm{max}} = M_{\mathrm{TOV}}(1 + \alpha P^{\beta}), \qquad (2)$$

and M_{TOV} is the maximum NS mass for a non-rotating NS, P is the spin period of the NS in units of second, and α and β are functions of M_{TOV}, NS radius (R), and moment of inertia (I).

For a given EoS, if its M_{TOV} is only slightly smaller than M_{ur}, it is possible that $M_{\mathrm{max}} > M_{\mathrm{ur}}$. In this case, the uniformly rotating remnant would be a supramassive NS. With the NS spinning down, the supramassive NS would collapse to a BH when M_{max} becomes smaller than M_{ur}. For an extremely stiff EoS, if $M_{\mathrm{TOV}} > M_{\mathrm{ur}}$, the merger remnant could even be a stable NS that never collapses.

For the purpose of this work, we adopt a series of NS EoSs with a range of maximum mass that allows $M_{\mathrm{max}} > 2.59\,M_{\odot}$, including three new unified NS EoSs (DD2, DDME2, and NL3$\omega\rho$) recently proposed (Fortin et al. 2016).[11] The numerical values of these EoSs for P_k (Kepler period), M_{TOV}, R, I, and the secondary parameters α and β are collected in Table 1, from calculations using the general relativistic NS equilibrium code RNS (Lasky et al. 2014; Li et al. 2016, 2017a). For the cases with $M_{\mathrm{TOV}} < 2.59\,M_{\odot}$, we calculate their NS collapsing period (P_{col}) by setting $M_{\mathrm{max}} = 2.59\,M_{\odot}$. We can see that for most EoSs (except for EoS NL3$\omega\rho$), P_{col} is very close to P_k, which are both of the order $\sim$1 ms. Notice that the adopted NS EoSs could all fulfill

---

[11] The same exercise may be performed to some quark star equations of state (e.g., Li et al. 2016; Zhou et al. 2017). On the other hand, if quark matter is stable, merging double quark stars would not produce the bright transient AT2017gfo as observed. We do not discuss these models in detail in this work.

Table 1
Basic Parameters for Adopted Equations of State

	$M_{\rm TOV}$ ($M_\odot$)	R_s (km)	I (10^{45} g cm^2)	α (s$^{-\beta}$)	β	P_K (ms)	$P_{\rm col}(\delta = 0.95,$ $M_{\rm ej} = 0.02\,M_\odot)$ (ms)	$P_{\rm col}(\delta = 1,$ $M_{\rm ej} = 0.01\,M_\odot)$ (ms)	$P_{\rm col}(\delta = 0.9,$ $M_{\rm ej} = 0.04\,M_\odot)$ (ms)
GM1	2.37	12.05	3.33	1.58×10^{-10}	-2.84	0.72	0.82	CD[a]	1.30
BSk21	2.28	11.08	4.37	2.81×10^{-10}	-2.75	0.60	0.70	CD[a]	0.90
DD2	2.42	11.89	5.43	1.370×10^{-10}	-2.88	0.65	0.95	0.77	2.40
DDME2	2.48	12.09	5.85	1.966×10^{-10}	-2.84	0.66	1.20	0.86	NC[b]
NL3$\omega\rho$	2.75	12.99	7.89	1.706×10^{-10}	-2.88	0.69	NC[b]	NC[b]	NC[b]

Notes.
[a] CD means collapse directly when the collapse period is smaller than Kepler period.
[b] NC means never collapse when the mass of uniform rotation is smaller than $M_{\rm TOV}$.

the limit on tidal deformability obtained from GW170817 (see details in discussion section).

3. Constraints from the Post-merger GW Signal

During the uniform rotation stage, the newly formed NS could lose its rotation energy through both magnetic dipole radiation and GW emission (Shapiro et al. 1983; Zhang & Mészáros 2001),

$$\dot{E} = I\Omega\dot{\Omega} = -L_{\rm sd,GW} - L_{\rm sd,EM}, \qquad (3)$$

where

$$L_{\rm sd,EM} = \frac{B_p^2 R^6 \Omega^4}{6c^3} \qquad (4)$$

is the magnetic dipole spin-down power, and

$$L_{\rm sd,GW} = \frac{32GI^2\epsilon^2\Omega^6}{5c^5} \qquad (5)$$

is the GW radiation spin-down power. $\Omega = 2\pi/P$ is the angular frequency and $\dot{\Omega}$ is its time derivative, ϵ is the ellipticity of the NS, and B_p is the dipolar field strength at the magnetic poles on the NS surface.

The characteristic amplitude of GWs from a rotating NS can be estimated as (Corsi & Mészáros 2017)

$$h_c = fh(t)\sqrt{\frac{dt}{df}}, \qquad (6)$$

where

$$h(t) = \frac{4G\Omega^2}{c^4 d}I\epsilon, \qquad (7)$$

with $f = \Omega/\pi$ representing the frequency of GW signals.

For a millisecond NS, the spin-down process could be dominated by the GW radiation, as long as ϵ is large enough. In

Table 2
The Characteristic Amplitude of GW Radiation h_c and its Upper Limit

	GM1	BSk21	DD2	DDME2	NL3$\omega\rho$
$h_c(\bar{f})(10^{-21})$	1.873	2.340	2.384	2.372	2.15
$h_{\rm c,upper}(\bar{f})(10^{-20})$	8.358	8.529	4.922	3.918	1.599

this case, we have $\dot{E} = -\frac{32GI^2\epsilon^2\Omega^6}{5c^5}$. Thus, we obtain

$$h_c = \sqrt{\frac{5IG}{Pc^3 d^2}}. \qquad (8)$$

The observation of GWs from the post-merger remnant by the LIGO-Virgo collaboration has given an upper limit strain as $h_{\rm rss}^{50\%} = 5.9 \times 10^{-22}$ Hz$^{-1/2}$ for a bar-mode model. With the definition of $h_{\rm rss}$, i.e.,

$$h_{\rm rss} = \left[2\int_{f_{\rm min}}^{f_{\rm max}} (|\widetilde{h}_+(f)|^2 + |\widetilde{h}_\times(f)|^2)df\right]^{1/2}, \qquad (9)$$

the relation between h_c and $h_{\rm rss}$ can be roughly derived by

$$h_c(\bar{f}) = h_{\rm rss}\frac{\bar{f}}{\sqrt{2(f_{\rm max} - f_{\rm min})}}, \qquad (10)$$

where $\bar{f} = (f_{\rm max} + f_{\rm min})/2$ is the average value of the GW frequency and $f_{\rm max}$ and $f_{\rm min}$ correspond to the Keplerian period P_k and the collapsing period $P_{\rm col}$, respectively. We choose the Keplerian period as the initial spin period of the merger product, so that $\Omega_0 = 2\pi/P_k$ is adopted.

With Equations (3)–(10), we derive the upper limits of $h_c(\bar{f})$ from the GW observation and the theoretical values of $h_c(\bar{f})$ for the adopted EoSs, assuming that the NS spin down is dominated by the GW radiation. The inferred results are shown in Table 2. We find that for all the adopted EoSs, the theoretical value of $h_c(\bar{f})$ is about one order of magnitude smaller than the observational upper limit, which indicates that even if the merger remnant of GW170817 is a millisecond massive NS, and the rotation energy of the NS is taken away by the GW radiation, the post-merger GW signal is undetectable. GW observations cannot

	GM1	BSk21	DD2	DDME2	NL3$\omega\rho$
			$\xi = 0.1$		
$\epsilon = 10^{-3}$	8.13×10^{13}	1.70×10^{14}	4.79×10^{13}	2.70×10^{13}	1.58×10^{12}
$\epsilon = 10^{-4}$	6.92×10^{11}	1.55×10^{12}	4.47×10^{11}	3.63×10^{11}	1.58×10^{11}
$\epsilon = 10^{-5}$	3.16×10^{10}	3.24×10^{10}	3.02×10^{10}	2.95×10^{10}	2.63×10^{10}
$\epsilon = 10^{-6}$	2.95×10^{10}	2.63×10^{10}	2.45×10^{10}	2.45×10^{10}	2.14×10^{10}
$\epsilon = 10^{-7}$	3.02×10^{10}	2.63×10^{10}	2.45×10^{10}	2.45×10^{10}	2.14×10^{10}
			$\xi = 1$		
	GM1	BSk21	DD2	DDME2	NL3$\omega\rho$
$\epsilon = 10^{-3}$	2.57×10^{13}	5.37×10^{13}	1.51×10^{13}	8.51×10^{12}	5.01×10^{11}
$\epsilon = 10^{-4}$	2.19×10^{11}	4.90×10^{11}	1.41×10^{11}	1.15×10^{11}	5.01×10^{10}
$\epsilon = 10^{-5}$	1.00×10^{10}	1.02×10^{10}	9.55×10^{9}	9.33×10^{9}	8.32×10^{9}
$\epsilon = 10^{-6}$	9.33×10^{9}	8.32×10^{9}	7.76×10^{9}	7.76×10^{9}	6.76×10^{9}
$\epsilon = 10^{-7}$	9.33×10^{9}	8.32×10^{9}	7.76×10^{9}	7.76×10^{9}	6.76×10^{9}

help to differentiate which power dominates the NS spin-down process, nor make any constraints on the ellipticity (ϵ) of the nascent NS.[12] In the following, we separately discuss different situations with ϵ ranging from 10^{-7} to 10^{-3}.

4. Constraints from EM Observations

4.1. Constraints from UV/optical/NIR Observations

If the merger remnant of GW170817 is a massive NS, the merger ejecta would be heated and accelerated by two different energy sources: r-process related radioactivity and dipole radiation from the NS. Due to energy conservation, we have (Yu et al. 2013)

$$\frac{dE}{dt} = \xi L_{\rm sd,EM} + \mathcal{D}^2 L_{\rm ra}' - \mathcal{D}^2 L_e', \qquad (11)$$

where E is the total energy of the ejecta, ξ represents the fraction of dipole radiation power injected into the ejecta, $L_{\rm ra}'$ is the comoving radioactive power, L_e' represents the comoving emitted bolometric luminosity, and $\mathcal{D} = 1/[\Gamma(1 - \beta)]$ is the Doppler factor, where β is the ejecta velocity in the lab frame and Γ is the corresponding bulk Lorentz factor. Here, we adopt the empirical expression for $L_{\rm ra}'$ proposed by Korobkin et al. 2012,

$$L_{\rm ra}' = 4 \times 10^{49} M_{\rm ej,-2} \left[\frac{1}{2} - \frac{1}{\pi} \arctan\left(\frac{t' - t_0'}{t_\sigma'} \right) \right]^{1.3} \text{ erg s}^{-1}, \qquad (12)$$

where $t_0' \sim 1.3$ s and $t_\sigma' \sim 0.11$ s. L_e' could be estimated by

$$L_e' = \begin{cases} \dfrac{E_{\rm int}' c}{\tau R_{\rm ej}/\Gamma}, & \tau > 1, \\[2ex] \dfrac{E_{\rm int}' c}{R_{\rm ej}/\Gamma}, & \tau < 1. \end{cases} \qquad (13)$$

$R_{\rm ej}$ is the radius of the ejecta in the lab frame, $\tau = \kappa (M_{\rm ej}/V')(R_{\rm ej}/\Gamma)$ is the optical depth of the ejecta with κ being the opacity (Kasen & Bildsten 2010; Kotera

et al. 2013), and $E_{\rm int}'$ is the internal energy in the comoving frame. The evolution of $E_{\rm int}'$ could be expressed as (Yu et al. 2013)

$$\frac{dE_{\rm int}'}{dt'} = \xi_t \mathcal{D}^{-2} L_{\rm d} + L_{\rm ra}' - L_e', -\mathcal{P}' \frac{dV'}{dt'}, \qquad (14)$$

with the radiation dominated pressure $\mathcal{P}' = E_{\rm int}'/3V'$ and the thermalization coefficient $\xi_t = \xi e^{-1/\tau}$. The comoving volume evolution can be fully addressed by $dV'/dt' = 4\pi R_{\rm ej}^2 \beta c$ and $dR_{\rm ej}/dt = \beta c/(1 - \beta)$.

The dynamic equation for the ejecta could be expressed as (Yu et al. 2013)

$$\frac{d\Gamma}{dt} = \frac{\frac{dE}{dt} - \Gamma \mathcal{D} \left(\frac{dE_{\rm int}'}{dt'} \right) - (\Gamma^2 - 1) c^2 \left(\frac{dM_{\rm sw}}{dt} \right)}{M_{\rm ej} c^2 + E_{\rm int}' + 2\Gamma M_{\rm sw} c^2}, \qquad (15)$$

where $M_{\rm sw} = \frac{4\pi}{3} R_{\rm ej}^3 n m_p$ is the shock swept mass of a medium with density n.

With Equations (11) to (15), one can easily solve the ejecta dynamics and the bolometric luminosity evolution of the ejecta thermal emission (L_e), and compare them with the observational data at the epoch when the observations were carried out (data provided in Drout et al. 2017). Given the tight allowed range of the spin period of the massive NS, the observations could place tight constraints on the dipole magnetic field strength of the NS (B_p). The results are collected in Table 3. We find that to be compatible with the UV/optical/NIR observations, if the merger remnant of GW170817 is a massive NS, the dipole magnetic field of the NS should be less than $\sim 10^{10}$–10^{11} G (see Figures 1 and 2).

Although no direct simulation results provide the exact value for the fraction of the dipole radiation power injected into the ejecta, ξ, a relatively large fiducial number was applied in the previous works (Yu et al. 2013; Metzger & Piro 2014), e.g., $0.1 < \xi < 1$. Next, we test two different cases with $\xi = 0.1$ and $\xi = 1$. We find that increasing ξ by one order of magnitude could tighten the constraint on B_p by a factor of three. We also test different situations with ϵ ranging from 10^{-7} to 10^{-3}. We find that as long as ϵ is smaller than 10^{-5}, different ϵ no longer affects the constraints on B_p. However, when ϵ is of the order $\sim 10^{-4}$, the constraint on B_p would become looser by one order of magnitude. When ϵ is of the order $\sim 10^{-3}$, the constraint on

---

[12] The ellipticity of a supramassive or stable NS can be induced either by a strong magnetic field or a rapid spin (e.g., Haskell et al. 2008; Frieben & Rezzolla 2012).
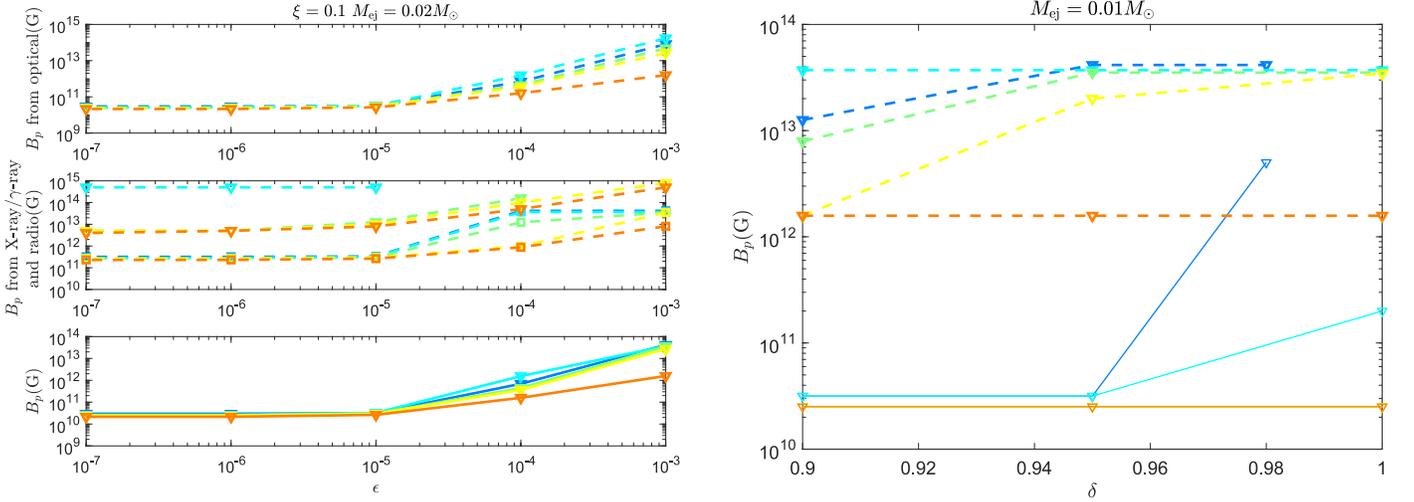
Figure 1. Constraints on the dipole magnetic field of the central NS from multi-band observations for $\xi = 0.1$ situation. Left panels: the top panel shows constrained results from UV/optical/NIR data. Constrained results from γ-ray/X-ray (marked with squares) and radio (marked with triangles) data are shown in the middle panel. The bottom panel shows the final results from multi-band data. Different colors correspond to different EoSs. Middle panel: the variation of final constraints with the mass fraction of core (δ) where $M_{\rm ej} = 0.01\,M_\odot$ is adopt. Right panel: the variation of final constraints with the mass of ejecta ($M_{\rm ej}$) where $\delta = 0.95$ is adopted. In the middle and right panels, the dashed and solid lines represent $\epsilon = 10^{-3}$ and $\epsilon = 10^{-5}$, respectively.
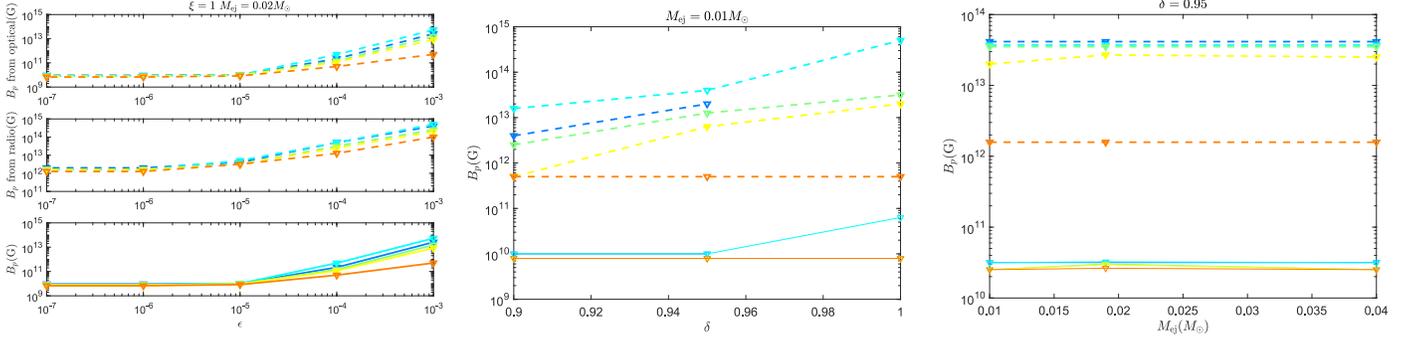

Figure 2. Constraints on the dipole magnetic field of the central NS from multi-band observations for $\xi = 1$ situation. Descriptions for each panels are the same with Figure 1.

B_p would become looser by two to three orders of magnitude. This is mainly because the high GW emission power could rapidly slow down the NS and drive it collapse into a BH.

4.2. Constraints from γ-Ray and X-Ray Observations

If the merger remnant of GW170817 is a massive NS, after the relativistic jet punches through the ejecta shell, the Poynting-flux outflow from the NS could leak out to power an extended emission. For GRB 170817A, Zhang et al. (2018) conducted a search of extended emission before and after the trigger time, which leads to a negative result. In this case, the γ-ray luminosity powered by the NS wind dissipation should not be larger than the luminosity of GRB 170817A, i.e., $\eta_\gamma L_{\rm sd,EM} \lesssim 1.7 \times 10^{47}\,{\rm erg\,s}^{-1}$.

On the other hand, when the ejecta becomes transparent, if the central NS has not collapsed, the dissipated photons from the NS wind would eventually diffuse out. Late time X-ray observations could serve as the upper limit of the X-ray luminosity powered by the NS wind dissipation, i.e., $\eta_x L_{\rm sd,EM}(t)e^{-\tau} \lesssim L_X(t)$. Here, we take the X-ray data (including upper limit) from Troja et al. (2017) to make constraints on the dipole magnetic field of the central NS. The constrained results for different EoSs have been collected in Table 4. We find that to be compatible with the γ-ray and X-ray

observations, if the merger remnant of GW170817 is a massive NS, the dipole magnetic field of the NS should be less than $\sim 10^{11}$–$10^{12}\,{\rm G}$ (see Figure 1), similar to the constraints from UV/optical/NIR data.

To be conservative, here we adopt a relatively small efficiency factor ($\eta_X = 10^{-4}$) to convert the spin-down luminosity to the observed X-ray luminosity (Xiao & Dai 2017), which is much smaller than the inferred value from previous investigations for a sample of short GRB X-ray plateau data (Zhang 2013; Rowlinson et al. 2014; Lü et al. 2015; Gao et al. 2016). Adopting a larger value of η_X would lead to much tighter constraints on B_p, which may fall below $10^{10}\,{\rm G}$. Note that because the observed γ-ray luminosity is much larger than the X-ray data, even assuming $\eta_X = 10^{-4}$ and $\eta_\gamma = 1$, the constraints on B_p are mainly from X-rays instead of γ-rays. The reason we only present the result for $\eta_X = 10^{-4}$ is as follows: suppose that the emission from Poynting-flux dissipation follows the synchrotron radiation spectrum. As the X-ray luminosity is much lower than that of GRB prompt emission, the νF_ν peak should be below the γ-ray band. Let us consider the extreme case where the peak is in the γ-ray band, so that $\eta_\gamma = 1$, and the X-ray and gamma-ray bands would be in the $\nu^{1/3}$ regime. One would have $\eta_\gamma \sim 10^4 \eta_X$ and hence, $\eta_X \sim 10^{-4}$, as $\eta_\nu \propto \nu F_\nu$ and the

Table 4
The Constrained Results on B_p from X-Ray/γ-Ray Observations

	GM1	BSk21	DD2	DDME2	NL3$\omega\rho$
$\xi = 0.1$, $\eta_X = 10^{-4}$					
$\epsilon = 10^{-3}$	4.15×10^{13}	3.71×10^{13}	3.52×10^{13}	3.45×10^{13}	8.13×10^{12}
$\epsilon = 10^{-4}$	4.15×10^{13}	3.71×10^{13}	1.23×10^{13}	9.55×10^{11}	8.71×10^{11}
$\epsilon = 10^{-5}$	3.31×10^{11}	3.16×10^{11}	2.95×10^{11}	2.95×10^{11}	2.63×10^{11}
$\epsilon = 10^{-6}$	3.16×10^{11}	2.82×10^{11}	2.63×10^{11}	2.63×10^{11}	2.29×10^{11}
$\epsilon = 10^{-7}$	3.16×10^{11}	2.82×10^{11}	2.63×10^{11}	2.63×10^{11}	2.29×10^{11}

Table 5
The Constrained Results on B_p(G) from Radio Observation

	GM1	BSk21	DD2	DDME2	NL3$\omega\rho$
$\xi = 0.1$, $n = 0.1$ cm^{-3}, $\epsilon_e = 0.1$, $\epsilon_B = 0.1$					
$\epsilon = 10^{-3}$	$\cdots$	$\cdots$	$\cdots$	9.55×10^{14}	5.01×10^{14}
$\epsilon = 10^{-4}$	$\cdots$	$\cdots$	1.70×10^{14}	1.15×10^{14}	5.25×10^{13}
$\epsilon = 10^{-5}$	$\cdots$	5.13×10^{14}	1.40×10^{13}	1.00×10^{13}	7.94×10^{12}
$\epsilon = 10^{-6}$	$\cdots$	5.13×10^{14}	5.89×10^{12}	5.50×10^{12}	5.01×10^{12}
$\epsilon = 10^{-7}$	$\cdots$	5.13×10^{14}	5.62×10^{12}	5.50×10^{12}	4.90×10^{12}
$\xi = 1$, $n = 0.1$ cm^{-3}, $\epsilon_e = 0.1$, $\epsilon_B = 0.1$					
$\epsilon = 10^{-3}$	4.17×10^{14}	5.37×10^{14}	3.02×10^{14}	2.45×10^{14}	1.10×10^{14}
$\epsilon = 10^{-4}$	5.13×10^{13}	6.03×10^{13}	3.39×10^{13}	2.69×10^{13}	1.32×10^{13}
$\epsilon = 10^{-5}$	4.37×10^{12}	5.62×10^{12}	3.31×10^{12}	3.39×10^{12}	3.16×10^{12}
$\epsilon = 10^{-6}$	2.18×10^{12}	1.91×10^{12}	1.82×10^{12}	1.78×10^{12}	1.26×10^{12}
$\epsilon = 10^{-7}$	2.14×10^{12}	1.86×10^{12}	1.78×10^{12}	1.74×10^{12}	1.26×10^{12}

frequency of gamma-rays is roughly 10^3 higher than that of X-rays.

Here, we only consider the $\xi = 0.1$ case.[13] We test different situations with ϵ ranging from 10^{-7} to 10^{-3}. Similar to the constrained results from UV/optical/NIR data, we find that different ϵ values do not affect the constrained results significantly, unless the GW emission power is large enough and rapidly drives the NS to collapse into a BH (when ϵ is around 10^{-4} or 10^{-3}). In these cases, the constraint on B_p becomes much looser because it is solely based on the γ-ray data.

4.3. Constraints from Radio Observations

Energy injection from the central NS, if exists, could significantly accelerate the ejecta. As long as the kinetic energy of the ejecta is large enough, the forward shock into the ambient medium could give rise to strong afterglow emission, at least in the radio band. The afterglow emission should not outshine the late radio observations, which could make further constraints on the dipole magnetic field of the central NS.

Within such an approach, the radio flux would be evidently affected by the parameters of ϵ_e, ϵ_B and n. Here, we present the constraint results for $p = 2.1$, $\epsilon_e = 0.1$, $\epsilon_B = 0.1$, and $n = 0.1$ cm^{-3}. We find that if the merger remnant of GW170817 is a long-lived NS, the dipole magnetic field of the NS should be less than $\sim 10^{12}$–10^{14} G (see Figure 1) to be compatible with the radio observations. The constrained results are shown in Table 5. Even for such an extreme parameter

regime, the radio data still cannot give tighter constraints than those given by optical and X-ray/gamma-ray. In reality, both ϵ_B and n should be much smaller and the constraint from radio data would be even looser.

Here, we consider two cases with $\xi = 0.1$ and $\xi = 1$. Again, we find that increasing ξ by one order of magnitude could tighten the constraint on B_p by a factor of 3. We also test different situations with ϵ values. We find that when $\epsilon \sim 10^{-3}$, the B_p upper limit is of the order $\sim 10^{14}$ G. When $\epsilon \sim 10^{-4}$, the B_p upper limit is of the order $\sim 10^{13}$ G. When ϵ is equal to or less than 10^{-5}, it no longer affects the constrained results on B_p, and the B_p upper limit is of the order $\sim 10^{12}$ G.

4.4. Summary of Quantitative Constraints

Combining all the constraints from GW and multi-band EM observations, we find that if the merger remnant of GW170817 is a massive NS, the NS should have a millisecond spin period, but a relatively low dipole magnetic field (B_p as low as $\sim 10^{10}$ G). The ellipticity of the NS is hardly constrained. If the ellipticity could reach 10^{-3}, B_p is constrained to the level of $\sim 10^{14}$ G. Otherwise, B_p is limited to the level of $\sim 10^9$–10^{11} G. These conclusions weakly depend on the adoption of NS EoSs. Specifically, for GM1, the upper limit of spin period is 0.82 ms and the upper limit of B_p is 9.33×10^9 G. For Bsk21, the upper limit of the spin period is 0.70 ms and the upper limit of B_p is 8.32×10^9 G. For DD2, the upper limit of spin period is 0.95 ms and the upper limit of B_p is 7.76×10^9 G. For DDME2, the upper limit of spin period is 1.20 ms and the upper limit of B_p is 7.76×10^9 G. For NL3$\omega\rho$, no upper limit of spin period could be given, and the upper limit of B_p is 6.76×10^9 G. Final constrained results are collected in Table 6. We also take the uncertainties of $M_{\rm ej}$ and δ into

---

[13] In the $\xi \sim 1$ case, no constraint on the spin-down luminosity could be made from X-ray and γ-ray observations, because almost all the spin-down power has been injected into the ejecta.

Table 6
Final Constrained Results on B_p(G)

	GM1	BSk21	DD2	DDME2	NL3$\omega\rho$
$\xi = 0.1$					
$\epsilon = 10^{-3}$	4.15×10^{13}	3.71×10^{13}	3.52×10^{13}	2.70×10^{13}	1.58×10^{12}
$\epsilon = 10^{-4}$	6.92×10^{11}	1.55×10^{12}	4.47×10^{11}	3.63×10^{11}	1.58×10^{11}
$\epsilon = 10^{-5}$	3.16×10^{10}	3.24×10^{10}	3.02×10^{10}	2.95×10^{10}	2.63×10^{10}
$\epsilon = 10^{-6}$	2.95×10^{10}	2.63×10^{10}	2.45×10^{10}	2.45×10^{10}	2.14×10^{10}
$\epsilon = 10^{-7}$	3.02×10^{10}	2.63×10^{10}	2.45×10^{10}	2.45×10^{10}	2.14×10^{10}
$\xi = 1$					
	GM1	BSk21	DD2	DDME2	NL3$\omega\rho$
$\epsilon = 10^{-3}$	2.57×10^{13}	5.37×10^{13}	1.51×10^{13}	8.51×10^{12}	5.01×10^{11}
$\epsilon = 10^{-4}$	2.19×10^{11}	4.90×10^{11}	1.41×10^{11}	1.15×10^{11}	5.01×10^{10}
$\epsilon = 10^{-5}$	1.00×10^{10}	1.02×10^{10}	9.55×10^{9}	9.33×10^{9}	8.32×10^{9}
$\epsilon = 10^{-6}$	9.33×10^{9}	8.32×10^{9}	7.76×10^{9}	7.76×10^{9}	6.76×10^{9}
$\epsilon = 10^{-7}$	9.33×10^{9}	8.32×10^{9}	7.76×10^{9}	7.76×10^{9}	6.76×10^{9}

consideration and find that the final constrained results are not sensitive to these two parameters. With the increase of δ, the final constraints become looser because the NS would collapse in a shorter timescale with a larger mass. For some soft EoSs (such as GM1 and Bsk21), if the mass of the core is larger than their $M_{\max}$, a uniformly rotating NS could never exist.

4.5. Other Constraints

Some other information may also pose constraints on the merger product. However, because they depend on complicated physical factors, an quantitative constraint is not easy to achieve. Nonetheless, it is worth discussing these factors qualitatively.

The first factor is the inferred mass and velocity of the ejecta. Fitting the optical/IR data of GW170817 led to an estimate of the mass, velocity, and opacity of both the blue and red components (Metzger 2017, for a review). However, it is unclear which component originates from the dynamical ejecta and which originates from a neutrino-driven wind (e.g., Gao et al. 2017a). It was proposed (Metzger et al. 2018) that a rapidly spinning HMNS with an ordered surface magnetic field strength of $\sim 10^{14}$ G and extended lifetime ($\sim$0.1–1 s) is required to simultaneously explain the velocity, total mass, and electron fraction of the blue component. It is hard to evaluate the consequence of a long-lived pulsar on the ejecta parameters. For the long-lived pulsar parameters constrained from the above quantitative analysis, usually a NS with a lower B_p is required. It may appear that the B field is too low to accelerate the ejecta to the desired velocity (due to the low spin-down luminosity). On the other hand, the longer lifetime of the pulsar would have a longer duration of energy injection into the ejecta, so that the fast velocity may be achievable. A long-lived pulsar may be questioned as it may over-eject mass due to a neutrino-driven wind from the surface of the NS. The neutrino-wind mass loss rate $\dot{M}_\nu \simeq 4 \times 10^{-4}\, M_\odot\, \mathrm{s}^{-1}$ $(L_\nu/2 \times 10^{52}\, \mathrm{erg\, s}^{-1})^{5/3}$ $(\epsilon_\nu/15\, \mathrm{MeV})^{10/3}$ $(M_{\mathrm{NS}}/2.4\, M_\odot)^{-2}$ $(R_{\mathrm{NS}}/15\, \mathrm{km})^{5/3}$ (Qian & Woosley 1996) has a strong dependence on the neutrino luminosity. Because the neutrino cooling timescale of a newborn NS is typically much shorter than the spin-down timescale of a low-field pulsar, a neutrino-driven wind mass would not be significantly larger than the HMNS case. The latter was found to be reasonable to account for the observation of AT2017gfo (Metzger et al. 2018).

Additional viscous mass ejection during the merger phase is expected. The predicted mass range is consistent with the inferred mass from the AT2017gfo (Radice et al. 2018).

Another constraint may come from the possible lanthanide abundance in the ejecta. The existence of a significant amount of lanthanides, as evidenced by the distinct "double-peaked" spectrum of AT2017gfo, may disfavor a strong magnetar wind, since such a wind would deeply ionize the lanthanides so that the opacity would be greatly reduced. However, our quantitative constraints favor a low-B pulsar, whose spin-down luminosity is low, so that the ionization flux may not be large enough to destroy lanthanides early on. The existence of lanthanides in the ejecta therefore may not pose great extra constraints to the pulsar parameters.

Finally, in the above analyses, we have taken ϵ and B_p as independent parameters. In principle, magnetic distortion may play the dominant role in creating and maintaining a relatively large ϵ for a newborn millisecond NS. Previous analytical and numerical studies suggest that within the magnetic distortion scenario, $\epsilon \propto B_p^2$ is usually invoked (Bonazzola & Gourgoulhon 1996b; Haskell et al. 2008). Recently, an ellipticity of the order $\epsilon \sim 0.005$ for a rapidly spinning (millisecond), strongly magnetized (10^{15} G), supramassive NS has been inferred from the statistical observational properties of Swift SGRBs (Gao et al. 2016). With such a normalization, the relation between ϵ and B_p can be then calibrated (Gao et al. 2017b). According to this relation, the above quantitative constraints for $\epsilon = 10^{-3}$ would be no longer relevant, as B_p is required to be in the level of 10^{15} G to achieve $\epsilon = 10^{-3}$. This is inconsistent with previous constrained results ($B_p < 10^{14}$ G). The quantitative constraints would be still valid if a different distortion mechanism other than magnetic distortion is at play (e.g., Frieben & Rezzolla 2012). For low ϵ value cases, since different ϵ values no longer affect the constrained results on B_p, the quantitative constraints discussed above still stand.

5. Conclusions and Discussions

The recent observations of GW170817 and its EM counterpart have opened a new era of GW-led multi-messenger astronomy. Comprehensive analyses of the multi-messenger information have provided some important physical properties of the compact objects and the merger process for GW170817. However, the remnant for the GW170817 merger remains

unknown. In this paper, we have investigated the possibility of a long-lived massive NS as the merger remnant of GW170817, and given constraints on the allowed physical properties of the NS, by invoking as much as available multi-messenger information as possible.

We found that there is no clear exclusion for a massive NS as the merger remnant of GW170817, but the parameter space for the newborn NS is limited. Constraints from GW and multi-band EM observations show that if the merger remnant of GW170817 is a massive NS, the NS should have a millisecond spin period, and a relatively low dipole magnetic field (as low as $\sim 10^{10}$ G). The ellipticity of the NS is hardly constrained. If the ellipticity reaches 10^{-3}, B_p is constrained to the level of $\sim 10^{14}$ G. Otherwise, B_p is limited to the level of $\sim 10^9$–10^{11} G. The conclusions weakly depend on the adoption of the NS EoS.

The constraints are mainly contributed by the UV/optical/ NIR and X-ray observations. The constraint from the current radio data is looser than the results from other bands. This result is based on the assumption that the radio signal is mainly generated by the ejecta-medium interaction forward shock. It is generally believed that the late time brightening signals in X-ray, optical, and radio bands are all contributed by the external dissipation of a structured jet (Lazzati et al. 2017; Troja et al. 2017, 2018; Margutti et al. 2018). If this is true, or if the radio signal starts to decay soon in the future (more than one hundred days after GW170817), or if Mooley et al. (2017) overestimated the kinetic energy of the ejecta, even more strict constraints may be placed on the NS properties.

In this paper, we considered five EoSs with a range of the maximum masses from $2.28\,M_\odot$ to $2.75\,M_\odot$. It has been shown that most of our adopted NS EoSs (GM1, BSk21, DD2, and DDME2) could fulfill the tight limit on tidal deformability $\Lambda(1.4\,M_\odot)$ of GW170817 under the prior of a low dimensionless NS spin (see Zhu et al. 2018, for details). Also, the possibility of NL3$\omega\rho$ EOS would not be clearly excluded if the high spin case is taken into account. This can be seen from its $\Lambda(1.4\,M_\odot)$ value of 925, which is below the 90% credible upper limit in the high spin case. The corresponding $\tilde{\Lambda}$ can be calculated as well, with the mass ratio range of GW170817 and a chirp mass equal to 1.188 solar mass. The resulting $\tilde{\Lambda}$ can actually be as small as 712 if the mass ratio of the system is 0.4 (which corresponds to the 90% credible range of the mass ratio in the high spin case for GW170817), that is very close to the 90% credible upper limit for $\tilde{\Lambda}$ in the high spin case. For NL3$\omega\rho$, we have $M_{\rm TOV} > 2.59\,M_\odot$. If such a EoS are valid, the merger remnant of GW170817 would be a stable NS that never collapses to a BH. For this case, there is no restriction on the spin period of the NS. In principle, if the spin period is extremely large (of the order ~ 100 ms), current EM observations would fail to give any constraint on the dipole magnetic field of the NS. However, because the newborn NS arises from the NS–NS merger scenario, the initial spin period should be close to 1 ms. Even with an extremely large ellipticity as $\epsilon \geqslant 0.001$, GW radiation cannot spin down the NS from 1 ms to 100 ms within a reasonable timescale. Even under this extreme EoS, the newborn NS is hardly possible to have a large B_p, unless some other mechanisms (e.g., r-mode instability, Andersson 1998; Lindblom et al. 1998; Dai et al. 2016) could somehow carry away its angular momentum at very early stage. For this EoS, we only consider dipole radiation and GW emission as the spin-down mechanism and take the Kepler period as the initial spin period.

Previous analyses on the short GRB data indicate that the dipole magnetic field of the merger producing NS is typically large ($\sim 10^{15}$ G; Rowlinson et al. 2014; Lü et al. 2015; Gao et al. 2016). If the central remnant of GW170817 is a massive NS, it is an outlier compared with other cases, but it is interesting to note that compared with other short GRBs, GRB 170817A is also an outlier in terms of luminosity.

For millisecond NSs, the detection horizons for the third-generation GW detectors, such as Einstein Telescope could reach 600 Mpc (Gao et al. 2017b). Future detections of the post-merger GW signals would be essential to determine NS– NS merger remnants and would further reveal the NS EoS.

Finally, we would like to point out two caveats of our approach. First, we take the Keplerian period as the initial spin period of the merger product. Strictly speaking, numerical simulations (Radice et al. 2018) showed that the initial period of the merger product is slightly longer than the Keplerian period, due to the strong viscous spin down during the merger phase. This phase also generates GWs that depend on the EoS. These complications are not considered. Second, in the real GW data analysis, the estimation of $h_{\rm rss}$ should be much more complicated. Our analytical derivation is only valid to order of magnitude, but is good enough for the purpose of this work.

ORCID iDs

Shunke Ai ⓘ https://orcid.org/0000-0002-9165-8312
He Gao ⓘ https://orcid.org/0000-0002-3100-6558
Zi-Gao Dai ⓘ https://orcid.org/0000-0002-7835-8585
Xue-Feng Wu ⓘ https://orcid.org/0000-0002-6299-1263
Ang Li ⓘ https://orcid.org/0000-0001-9849-3656
Bing Zhang ⓘ https://orcid.org/0000-0002-9725-2524

References

Abbott, B. P., Abbott, R., Abbott, T. D., et al. 2017a, PhRvL, 119, 161101
Abbott, B. P., Abbott, R., Abbott, T. D., et al. 2017b, ApJ, 848L, 12A
Abbott, B. P., Abbott, R., Abbott, T. D., et al. 2017c, ApJL, 851L, 16A
Andersson, N. 1998, ApJ, 502, 708
Arcavi, I., Hosseinzadeh, G., Howell, D. A., et al. 2017, Natur, 551, 64
Bauswein, A., Just, O., Janka, H.-T., & Stergioulas, N. 2017, ApJL, 850, L34
Bonazzola, S., & Gourgoulhon, E. 1996b, A&A, 312, 675
Bucciantini, N., Metzger, B. D., Thompson, T. A., & Quataert, E. 2012, MNRAS, 419, 1537
Chornock, R., Berger, E., Kasen, D., et al. 2017, ApJL, 848, L19
Corsi, A., & Mészáros, P. 2017, ApJ, 702, 1171
Coulter, D. A., Foley, R. J., Kilpatrick, C. D., et al. 2017, Sci, 358, 1556
Cowperthwaite, P. S., Berger, E., Villar, V. A., et al. 2017, ApJL, 848, L17
Dai, Z. G. 2004, ApJ, 606, 1000
Dai, Z. G., & Lu, T. 1998a, PhRvL, 81, 4301
Dai, Z. G., & Lu, T. 1998b, A&A, 333, L87
Dai, Z. G., Wang, S. Q., Wang, J. S., Wang, L. J., & Yu, Y. W. 2016, ApJ, 817, 13
Dai, Z. G., Wang, X. Y., Wu, X. F., & Zhang, B. 2006, Sci, 311, 1127
de Vaucouleurs, G., de Vaucouleurs, A., Corwin, H. G., Jr., et al. 1991, Third Reference Catalogue of Bright Galaxies (Vol. I, II, III; New York: Springer)

Drout, M. R., Piro, A. L., Shappee, B. J., et al. 2017, Sci, 358, 1570
Evans, P. A., Cenko, S. B., Kennea, J. A., et al. 2017, Sci, 358, 1565
Fan, Y.-Z., Yu, Y.-W., Xu, D., et al. 2013, ApJL, 779, L25
Fortin, M., Providência, C., Raduta, A. R., et al. 2016, PhRvC, 94, 035804
Frieben, J., & Rezzolla, L. 2012, MNRAS, 427, 3406
Gao, H., Cao, Z., Ai, S., & Zhang, B. 2017a, ApJL, 851, L45
Gao, H., Cao, Z., & Zhang, B. 2017b, ApJL, 844, 112
Gao, H., Ding, X., Wu, X.-F., Dai, Z.-G., & Zhang, B. 2015, ApJ, 807, 163
Gao, H., Ding, X., Wu, X.-F., Zhang, B., & Dai, Z.-G. 2013, ApJ, 771, 86
Gao, H., Zhang, B., & Lü, H.-J. 2016, PhRvD, 93, 044065
Goldstein, A., Veres, P., Burns, E., et al. 2017, ApJL, 848, L14
Gottlieb, O., Nakar, E., Piran, T., & Hotokezaka, K. 2017, arXiv:1710.05896
Hanauske, M., Takami, K., Bovard, L., et al. 2017, PhRvD, 96, 043004
Haskell, B., Samuelsson, L., Glampedakis, K., & Andersson, N. 2008, MNRAS, 385, 531
Kasen, D., & Bildsten, L. 2010, ApJ, 717, 245
Kasen, D., Metzger, B., Barnes, J., Quataert, E., & Ramirez-Ruiz, E. 2017, Natur, 551, 80
Kasliwal, M. M., Nakar, E., Singer, L. P., et al. 2017, Sci, 358, 1559
Kilpatrick, C. D., Foley, R. J., Kasen, D., et al. 2017, Sci, 358, 1583
Korobkin, O., Rosswog, S., Arcones, A., & Winteler, C. 2012, MNRAS, 426, 1940
Kotera, K., Phinney, E. S., & Olinto, A. V. 2013, MNRAS, 432, 3228
Lasky, P. D., Haskell, B., Ravi, V., et al. 2014, PhRvD, 89, 047302
Lazzati, D., Perna, R., Morsony, B. J., et al. 2017, arXiv:1712.03237
Li, A., Zhang, B., Zhang, N.-B., et al. 2016, PhRvD, 94, 083010
Li, A., Zhu, Z.-Y., & Zhou, X. 2017a, ApJ, 844, 41L
Li, L.-X., & Paczyński, B. 1998, ApJL, 507, 59L
Li, S.-Z., Liu, L.-D., Yu, Y.-W., & Zhang, B. 2017b, arXiv:1804.06597
Li, S.-Z., & Yu, Y.-W. 2016, ApJ, 819, 120
Lindblom, L., Owen, B. J., & Morsink, S. M. 1998, PhRvL, 80, 4843
Lü, H.-J., Zhang, B., Lei, W.-H., Li, Y., & Lasky, P. D. 2015, ApJ, 805, 89
Lyman, J. D., Lamb, G. P., Levan, A. J., et al. 2018, arXiv:1801.02669
Ma, P.-X., Jiang, J.-L., Wang, H., et al. 2017, ApJ, 858, 74
Margalit, B., & Metzger, B. D. 2017, ApJL, 850, L19
Margutti, R., Alexander, K. D., Xie, X., et al. 2018, ApJL, 856, L18
Meng, Y.-Z., Geng, J.-J., Zhang, B.-B., et al. 2018, arXiv:1801.01410
Metzger, B. D. 2017, ApJ, 856, 101
Metzger, B. D., Martínez-Pinedo, G., Darbha, S., et al. 2010, MNRAS, 406, 2605
Metzger, B. D., & Piro, A. L. 2014, MNRAS, 439, 3916
Metzger, B. D., Thompson, T. A., & Quataert, E. 2018, arXiv:1801.04286
Mooley, K. P., Nakar, E., Hotokezaka, K., et al. 2017, Natur, 554, 207
Nicholl, M., Berger, E., Kasen, D., et al. 2017, ApJL, 848, L18
Perego, A., Radice, D., & Bernuzzi, S. 2017, ApJL, 850, L37
Piro, A. L., & Kollmeier, J. A. 2017, ApJ, 855, 103
Qian, Y., & Woosley, S. E. 1996, ApJ, 471, 331
Radice, D., Perego, A., Bernuzzi, S., & Zhang, B. 2018, arXiv:1803.10865
Rezzolla, L., Most, E. R., & Weih, L. R. 2018, ApJL, 852, L25
Rowlinson, A., Gompertz, B. P., Dainotti, M., et al. 2014, MNRAS, 443, 1779
Ruiz, M., Shapiro, S. L., & Tsokaros, A. 2017, PhRvD, 97, 021501
Shapiro, S. L., Teukolsky, S. A., & Lightman, A. P. 1983, PhT, 36, 89
Shappee, B. J., Simon, J. D., & Drout, M. R. 2017, Sci, 358, 1574
Siegel, D. M., & Ciolfi, R. 2016a, ApJ, 819, 15
Siegel, D. M., & Ciolfi, R. 2016b, ApJ, 819, 14
Smartt, S. J., Chen, T.-W., Jerkstrand, A., et al. 2017, Natur, 551, 75
Sun, H., Zhang, B., & Gao, H. 2017, ApJ, 835, 7
Tanvir, N. R., Levan, A. J., González-Fernández, C., et al. 2017, ApJL, 848, L27
Troja, E., Piro, L., Ryan, G., et al. 2018, arXiv:1801.06516
Troja, E., Piro, L., van Eerten, H., et al. 2017, Natur, 551, 71T
Villar, V. A., Guillochon, J., Berger, E., et al. 2017, ApJL, 851, L21
Wu, X.-F., Gao, H., Ding, X., et al. 2014, ApJL, 781, L10
Xiao, D., & Dai, Z.-G. 2017, ApJ, 846, 130
Xiao, D., Liu, L.-D., Dai, Z.-G., & Wu, X.-F. 2017, ApJL, 850, L41
Yu, Y.-W., & Dai, Z.-G. 2017, arXiv:1711.01898
Yu, Y.-W., Zhang, B., & Gao, H. 2013, ApJ, 776, L40
Zhang, B. 2013, ApJ, 763, L22
Zhang, B., & Mészáros, P. 2001, ApJ, 552, L35
Zhang, B.-B., Zhang, B., Sun, H., et al. 2018, NatCo, 9, 447
Zhou, E., Zhou, X., & Li, A. 2017, PhRvD, 97, 083015
Zhu, Z.-Y., Zhou, E.-P., & Li, A. 2018, arXiv:1802.05510